Structure
Article

An Autoinhibited Conformation of LGN Reveals a Distinct Interaction Mode between GoLoco Motifs and TPR Motifs

Zhu Pan,[1,2,4] Jinwei Zhu,[1,2,4] Yuan Shang,[2,4] Zhiyi Wei,[2,3] Min Jia,[1] Caihao Xia,[1] Wenyu Wen,[1] Wenning Wang,[1,*] and Mingjie Zhang[2,3,*]
[1]Shanghai Key Laboratory of Molecular Catalysis and Innovative Materials, Department of Chemistry and Institutes of Biomedical Sciences, Fudan University, Shanghai, China
[2]Division of Life Science, State Key Laboratory of Molecular Neuroscience
[3]Center of Systems Biology and Human Health, School of Science and Institute for Advanced Study
Hong Kong University of Science and Technology, Clear Water Bay, Kowloon, Hong Kong, China
[4]These authors contributed equally to this work
*Correspondence: wnwang@fudan.edu.cn (W.W.), mzhang@ust.hk (M.Z.)
http://dx.doi.org/10.1016/j.str.2013.04.005

SUMMARY

LGN plays essential roles in asymmetric cell divisions via its N-terminal TPR-motif-mediated binding to mInsc and NuMA. This scaffolding activity requires the release of the autoinhibited conformation of LGN by binding of $G\alpha_i$ to its C-terminal GoLoco (GL) motifs. The interaction between the GL and TPR motifs of LGN represents a distinct GL/target binding mode with an unknown mechanism. Here, we show that two consecutive GL motifs of LGN form a minimal TPR-motif-binding unit. GL12 and GL34 bind to TPR0–3 and TPR4–7, respectively. The crystal structure of a truncated LGN reveals that GL34 forms a pair of parallel α helices and binds to the concave surface of TPR4–7, thereby preventing LGN from binding to other targets. Importantly, the GLs bind to TPR motifs with a mode distinct from that observed in the GL/$G\alpha_i$·GDP complexes. Our results also indicate that multiple and orphan GL motif proteins likely respond to G proteins with distinct mechanisms.

INTRODUCTION

Asymmetric cell division (ACD) is a fundamental process to generate cellular diversity during animal development (Cowan and Hyman, 2004; Gönczy, 2008; Knoblich, 2010; Morrison and Kimble, 2006; Neumüller and Knoblich, 2009; Siller and Doe, 2009). In ACD, cells establish a polarity axis to coordinate the polarized distribution of cell-fate determinants and orientation of the mitotic spindle, giving rise to two daughter cells with different cell fates. In mammals, an evolutionarily conserved protein complex, NuMA-LGN-$G\alpha_i$ (orthologs in *Drosophila*: Mud-Pins-$G\alpha_i$; orthologs in *C. elegans*: Lin5-GPR1,2-$G\alpha$), functions in a receptor-independent G protein signaling pathway to orient the mitotic spindle along the polarity axes of cells (Bowman et al., 2006; Couwenbergs et al., 2007; Izumi et al., 2006; Park and Rose, 2008; Siller et al., 2006; Yu et al., 2006). Through the interaction between the NuMA-LGN-$G\alpha_i$ complex and dynein, cortical localized dynein will then generate a pulling force on astral microtubules to move toward the minus end of microtubules, thus aligning the mitotic spindle with the cellular polarity axis (Couwenbergs et al., 2007; Kotak et al., 2012; Merdes et al., 1996; Nguyen-Ngoc et al., 2007; Siller and Doe, 2008; Siller et al., 2005; Williams et al., 2011; Yingling et al., 2008).

Recent studies have shown that a receptor-independent G protein signaling pathway plays essential roles in regulating the mitotic spindle positioning in different model systems. Unlike the canonical G protein signaling pathway, which is activated by the G-protein-coupled receptor (GPCR), the receptor-independent G protein signaling pathway in ACD is regulated by the cytosolic GoLoco (GL)-motif-containing protein LGN (Pins in *Drosophila* and GPR1,2 in *C. elegans*). The scaffold protein LGN contains eight N-terminal tetratricopeptide (TPR) motifs and four C-terminal GL motifs. Each of the four GL motifs can bind to heterotrimeric G-protein subunit $G\alpha_i$·GDP independent of each other and with high affinity (Parmentier et al., 2000; Schaefer et al., 2000, 2001). Binding of LGN to $G\alpha_i$·GDP can compete with $G\beta\gamma$ heterodimer, thus triggering the noncanonical G-protein signaling pathway (Yu et al., 2006). Recent biochemical and structural data further show that LGN can also act as a guanine nucleotide dissociation inhibitor (GDI) (Jia et al., 2012; McCudden et al., 2005).

Binding of LGN to $G\alpha_i$·GDP activates not only the noncanonical G protein signaling pathway but also LGN itself. LGN was found to function as a conformational switch via intramolecular interactions between its TPR motifs and GL motifs (Du and Macara, 2004; Nipper et al., 2007; Smith and Prehoda, 2011). $G\alpha_i$·GDP bound to LGN GL motifs may release the autoinhibited conformation, promoting binding of the N-terminal TPR motifs to their targets, including NuMA and mInsc. It was shown that Mud (*Drosophila* ortholog of NuMA) and $G\alpha_i$ bind to Pins (*Drosophila* ortholog of LGN) cooperatively, thus completely opening the autoinhibited conformation of Pins (LGN) (Du and Macara, 2004; Nipper et al., 2007). Biochemical study of the Pins intramolecular interaction demonstrated that not all three GL motifs are involved in the intramolecular interactions (Nipper et al., 2007). In

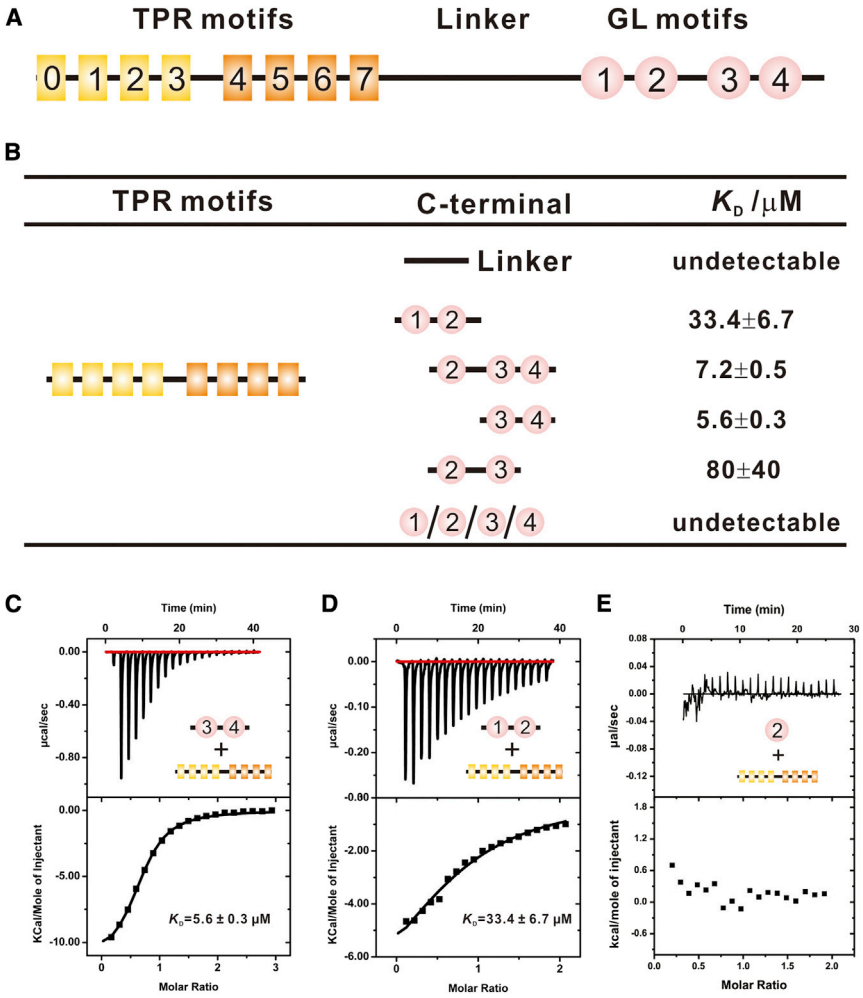

Figure 1. The LGN C-Terminal GL Motifs Form Two Pairs of GL Motif Tandems, Each Capable of Binding to the N-terminal TPR Motifs

(A) Schematic diagram of the domain organization of LGN.

(B) ITC-based binding affinities of various GL-motif fragments for TPR0–7 (residues 15–350). Note that two GL motifs connected in tandem (i.e., GL12 or GL34) can bind to TPR0–7, whereas individual GL motifs show no detectable binding to TPR0–7.

(C–E) Examples of ITC titration curves for the bindings between GL34 and TPR0–7 (C), GL12 and TPR0–7 (D), and GL2 and TPR0–7 (E).

contrast, all of the four LGN GL motifs were reported to be required for the interaction with N-terminal TPR motifs (Du and Macara, 2004). Thus, the activity of LGN and Pins may be differentially regulated due to the difference of their GL numbers. However, understanding of the regulation mechanism of this conformational switch is far from complete. It is not clear how GL motifs couple with TPR motifs in LGN or Pins and how the binding of $G\alpha_i$·GDP to GL motifs triggers the release of their autoinhibited conformation.

Combining biochemical and structural approaches, we have dissected the interaction between TPR motifs and GL motifs of LGN and found that each of the two tandem GL motifs (GL12, GL34) forms a minimal TPR-motif-binding module. The structure of a truncated LGN (TPR2–7-GL34) solved here reveals the molecular mechanism underlying the autoinhibition of LGN. We demonstrate that the binding of $G\alpha_i$·GDP to LGN can release the autoinhibited conformation of LGN and enhance the binding of TPR motifs to NuMA. We further show that multiple GL motifs bind to TPR motifs with a mode distinctly different from that observed for the single GL motif binding to $G\alpha_i$·GDP, which indicates that multiple GL motifs are likely to respond to the G protein signaling pathway with a distinct mechanism.

RESULTS

A Pair of GL Motifs Connected in Tandem Forms a Minimal TPR-Motif-Binding Unit

The C-terminal region of LGN contains four GL motifs (Figure 1A), each of which can bind to $G\alpha_i$·GDP with a K_d ~50–100 nM (Jia et al., 2012; McCudden et al., 2005). The eight TPR motifs (TPR0–7, amino acids [aa] 15–350) of LGN are responsible for its binding to NuMA and mInsc (Culurgioni et al., 2011; Yuzawa et al., 2011; Zhu et al., 2011). To understand the molecular mechanism of the autoinhibition of LGN, we set out to characterize in detail the biochemical bases of the interactions between the TPR motifs and GL motifs using various highly purified fragments of LGN (Figures 1B–1E). Unexpectedly, none of the individual GL motifs showed detectable binding to TPR0–7 (Figures 1B and 1E). Instead, a pair of GL motifs arranged in tandem (GL12 or GL34) showed specific binding to TPR0–7, and GL34 displayed a stronger binding to TPR0–7 than did GL12 (Figures 1B–1D). Extension of GL34 in its N-terminus by inclusion of GL2 did not enhance binding of GL34 to TPR0–7 (Figure 1B), indicating that a pair of GL motifs connected in tandem forms a minimal TPR-motif-binding unit. One would expect that the intramolecular interaction between TPR motifs and GL motifs of LGN is much stronger, given that TPR0–7 can bind to the two isolated tandem GL pairs (GL12 and GL34) with a K_d ranging from several to dozens of μM (Figure 1B). We could not perform a direct biochemical characterization of the interaction between TPR0–7 and GL1–4, as we were unable to obtain high quality GL1–4. As expected, the linker region (aa 374–479) that connects the TPR motifs and the GL motifs did not bind to TPR0–7 (Figure 1B).

GL12 and GL34 Bind to TPR0–7 Simultaneously

Having established that GL12 and GL34 can individually bind to TPR0–7 in *trans*, we next investigated whether the two GL tandems can bind to TPR0–7 simultaneously. To answer this question, we performed a series of quantitative binding competition assays. We found that the presence of an excess amount of

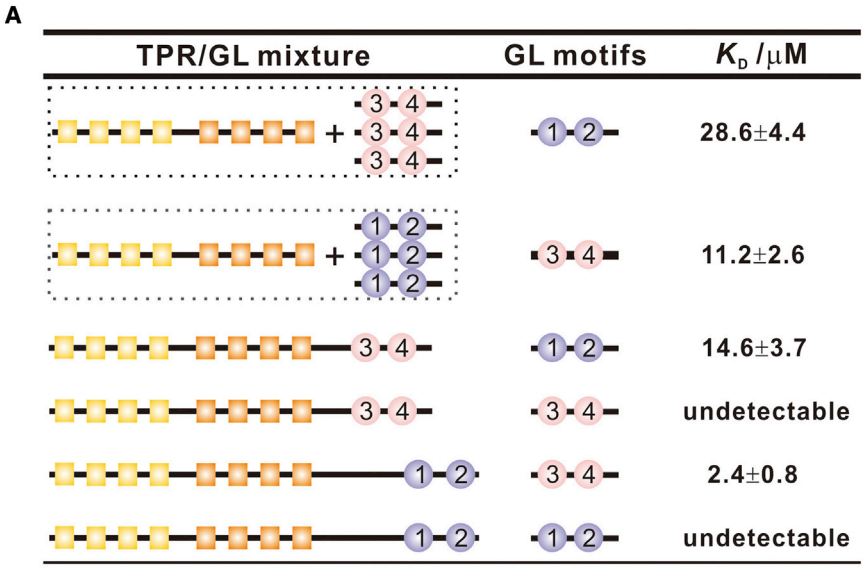

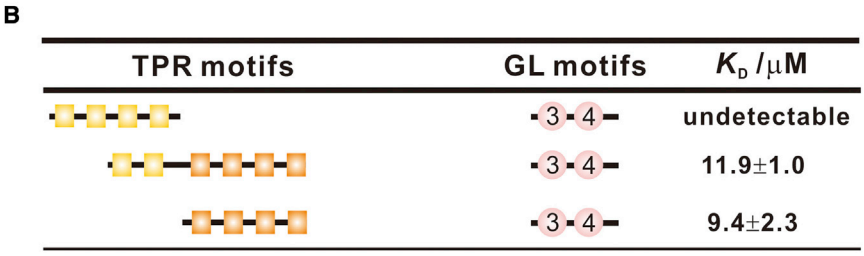

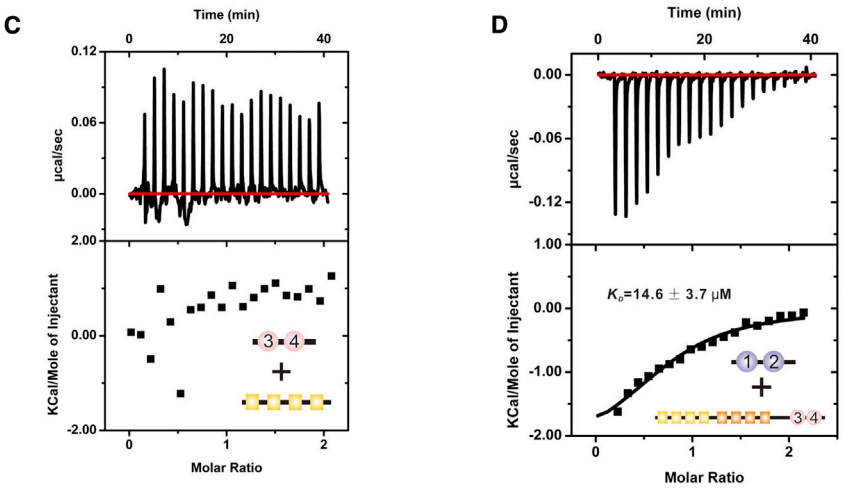

Figure 2. GL12 and GL34 Can Bind to TPR0–7 Simultaneously

(A) The top two rows show that the binding of GL12 (or GL34) to TPR0–7 is not affected by the presence of excess amount of GL34 (or GL12). The middle two rows show that fusion of GL34 at the C terminus of TPR0–7 effectively blocks GL34 but has no impact on GL12 binding to TPR motifs. The bottom two rows show that fusion of GL12 at the C terminus of TPR0–7 effectively blocks GL12 but has no impact on GL34 binding to TPR motifs.

(B–D) ITC-based binding affinities of various LGN TPR-motif fragments with GL34 (B), with representative ITC curves for binding of GL34 to TPR0–4 (C) and GL12 to TPR0–7-GL34 fusion protein (D).

GL34 (GL34:TPR0–7 molar ratio of ~3:1) did not affect the binding of GL12 to TPR0–7. Conversely, the presence of an excess amount of GL12 (GL12:TPR0–7 molar ratio of ~3:1) had a minor effect on the binding of GL34 to TPR0–7 (Figure 2A). The above set of experiments indicates that GL12 and GL34 can bind to TPR0–7 simultaneously. To further consolidate this conclusion, we used various fusion constructs to mimic the LGN intramolecular GL/TPR interaction. When TPR0–7 was fused with GL34, the resulting fusion protein (TPR0–7-GL34) can bind to GL12 effectively, with a binding affinity a little bit higher than that observed for TPR0–7 alone (Figures 2A and 2D). This TPR0–7-GL34 fusion protein showed no detectable interaction with GL34 (Figure 2A), presumably due to a much stronger intramolecular GL34/TPR0–7 interaction in the fused protein. In parallel, the TPR0–7-GL12 fusion protein showed a robust binding to GL34 but not to GL12 (Figure 2A). These data indicate that the GL12 and GL34 tandems bind to different regions of LGN TPR motifs.

To map the exact TPR motifs that are responsible for binding to GL12 and to GL34, we produced several LGN fragments containing various TPR motifs. We found that TPR4–7 (aa 191–350) binds to GL34 with an affinity comparable to that of TPR0–7 (Figure 2B). Inclusion of more TPR motifs (i.e., TPR2–7, aa 89–350) did not enhance the GL34 binding affinity of TPR4–7. Additionally, we could not detect binding between TPR0–3 (aa 15–194) and GL34 by an isothermal-titration-calorimetry (ITC)-based assay (Figures 2B and 2C). Considering the fact that GL12 and GL34 bind to different regions of TPR motifs together with all the mapping data, we propose that GL12 likely binds to the N-terminal half of TPR, which is consistent with the results from the mutagenesis experiments shown below. The finding that each of the two halves of the LGN TPR-motif unit is responsible for binding to one of the two GL tandems is consistent with our earlier finding that four TPR motifs of LGN form a target binding structural unit (Zhu et al., 2011).

Crystal Structure of the TPR2–7/GL34 Complex

To understand the molecular basis underlying GL-mediated autoinhibition of LGN, we attempted to crystallize the full-length LGN or complexes formed by various fragments of TPR motifs with different combinations of GL motifs. Among numerous combinations tested, we succeeded in obtaining crystals with

Table 1. Statistics of X-Ray Crystallographic Data Collection and Model Refinement

Data Collection	
Space group	$P22_12_1$
Unit Cell Parameters	
a, b, c (Å)	a = 72.213, b = 81.803, c = 106.942
Resolution range (Å)	50.00–2.80 (2.85–2.80)
No. of unique reflections	16256 (788)
Redundancy	6.9 (6.2)
I/σ(I)	21.6 (2.4)
Completeness (%)	99.9 (99.9)
R_{merge} (%)[a]	8.5 (64.6)
Wilson_B	73.9
Structure Refinement[b]	
Resolution (Å)	38.0–2.8 (3.0–2.8)
R_{cryst}[c]/R_{free}[d] (%)	25.1 (23.3)/31.1(32.2)
rmsd bonds (Å)/angles (°)	0.008/1.112
No. of Reflections	
Working set	15024
Test set	798
Protein atoms	4249
Average B factor (Å^2)	75.4
Ramachandran Plot	
Most favored regions (%)	97.4
Additionally allowed (%)	2.6
Generously allowed (%)	0

Numbers in parentheses represent values for the highest-resolution shell.
[a]$R_{merge} = \Sigma\ |Ii - <I>|/\Sigma Ii$, where Ii is the intensity of measured reflection and <I> is the mean intensity of all symmetry-related reflections.
[b]Refinement statistics were based on the data for $F/\sigma(F) > 2$.
[c]$R_{cryst} = \Sigma||F_{calc}| - |F_{obs}||/\Sigma F_{obs}$, where F_{obs} and F_{calc} are the observed and calculated structure factors.
[d]$R_{free} = \Sigma T||F_{calc}| - |F_{obs}||/\Sigma F_{obs}$, where T is a test data set of about 5% of the total unique reflections randomly chosen and set aside prior to refinement.

superior diffractions from a fusion protein in which GL34 was fused to the C-terminal tail of TPR2–7 (referred to hereafter as TPR2–7-GL34). The TPR2–7-GL34 structure was solved by molecular replacement using the structure of LGN-TPR4–7/mInsc as the search model (Zhu et al., 2011) (Table 1). Each asymmetric unit contains two copies of TPR2–7-GL34 that are covalently linked by two intermolecular disulfide bonds formed between Cys117 from αB of TPR2 and Cys597 from GL3 (Figure S1 available online). Given that TPR2 of LGN is not required for binding to GL34 (Figure 2), the observed intermolecular disulfide bond is likely to be a crystallization artifact. Nonetheless, formation of this disulfide bond might have facilitated the crystallization of TPR2–7-GL34, as we were not able to obtain crystals for other constructs (e.g., TPR4–7-GL34).

Except for the N-terminal 20 amino acids of TPR2–7 (residues 91–109, corresponding to αA of TPR2; Zhu et al., 2011), two amino acids connecting TPR2–7 and GL34, and a few residues in the αA/αB-linker of TPR motifs, the rest of the protein is well resolved (Figures 3A and S3). The conformation of the TPR motifs in TPR2–7-GL34 is very similar to that of the corresponding TPR motifs in the LGN-TPR0–7/NuMA complex structure (rmsd ~0.98 Å; Figure S2A). Entirely consistent with the biochemical data shown in Figures 1 and 2, GL3 and GL4 interact with each other to form an integral structural unit (i.e., the GL34 tandem), within which each motif (GL3 and GL4) forms an α-helix and the two helices are arranged in a parallel manner (Figures 3A and S3B). The GL34 tandem makes direct contact with the concave surface of TPR5–7 (Figures 3A and 3B). There is no contact between TPR23 and GL34. Except for a hydrogen bond between Y206 in TPR4 and E622 in GL4, no direct interaction between TPR4 and GL34 can be observed, suggesting that TPR4 likely functions to maintain the structural integrity of TPR4–7.

The interactions between TPR5–7 and GL34 are mediated by hydrophobic as well as polar interactions between conserved residues from both TPR motifs and the GL motifs (Figures 3B, 4E, and S3A). The highly conserved hydrophobic residues Phe624, Leu627, and Ile628 from GL4 interact with Ile246 and Phe247 from TPR5 and Thr286 and Leu287 from TPR6 (Figures 3B and S3A). Phe591, Leu594, and Val595 from GL3, Phe625 and Leu629 from GL4, and Trp319 from TPR7 form the second hydrophobic core of the complex. In addition to these hydrophobic interactions, extensive charge-charge and hydrogen-bonding interactions also contribute to the interaction between TPR5–7 and GL34 (Figures 3B and S3A). For example, the highly conserved Arg316 from TPR7-αA and Tyr279 from TPR6-αA form extensive hydrogen bonds with Asp587 and Asp589 from GL3 and Asp623 from GL4. Arg236 from TPR5-αA forms a salt bridge with Asp621 from GL4. It is noted that the majority of the GL34-interacting residues from TPR5–7 (e.g., Ile246, Phe247, Leu287, and Arg316) are also found to be critical for LGN to bind to NuMA or mInsc (Culurgioni et al., 2011; Yuzawa et al., 2011; Zhu et al., 2011), explaining how the GL-motif-mediated autoinhibited conformation of LGN can prevent NuMA or mInsc from binding.

We performed a series of mutagenesis experiments to verify the validity of the interactions observed from the structure of TPR2–7-GL34. We scanned through the entire concave surface of TPR0–7 by mutating the absolutely conserved Asn residues in the "Leu-Gly_Asn"-motif in the αB helix of each TPR motif. As shown in Figure 3C, substitutions of each Asn in TPR1–3 (Asn63 in TPR1, Asn103 in TPR2, and Asn143 in TPR3) with Glu had no impact on binding of GL34 to TPR0–7. In contrast, substitution of Asn283 in TPR6 and Asn323 in TPR7 with Glu invariably impaired TPR0–7 from binding to GL34. Similarly, substitutions of two conserved charged residues in TPR0–3 (Lys96 in TPR2 and Arg136 in TPR3) with Ala had no impact on the TPR0–7/GL34 interaction, whereas substitution of Asp310, which is in TPR7-αA and forms a hydrogen bond with Thr618 in the linker between GL3 and GL4, with Ala completely disrupted the interaction between TPR0–7 and GL34 (Figures 3B and 3C). Additionally, substitution of Phe591 from GL3 or Phe624 from GL4 with Glu also completely abolished binding of GL34 to TPR0–7 (Figure 3C), as both Phe residues are in the hydrophobic interface between TPR2–7 and GL34 (Figure 3B and S3A). Finally, we used a NuMA peptide to validate the structure of TPR2–7-GL34 further. According to our previous study of the LGN-TPR0–7/NuMA complex (Zhu et al., 2011), a shorter

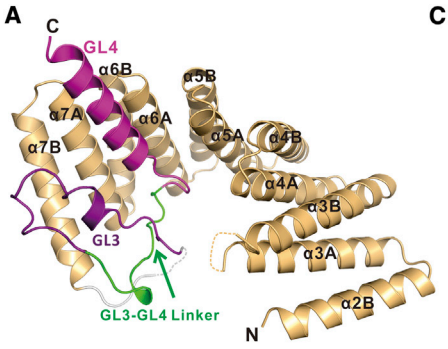

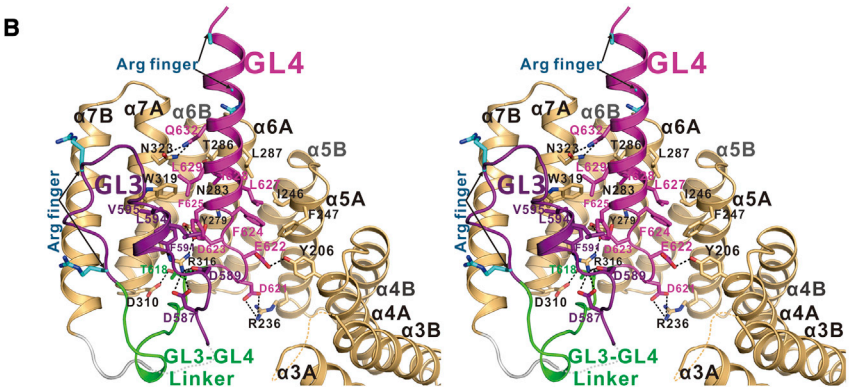

C

TPR0-7	K_D /μM	GL34	K_D /μM
WT	5.6±0.3		
N63E	4.3±0.6	F591E	undetectable
N103E	9.5±1.1	F624E	undetectable
N143E	5.7±0.8		
K96A,R136A	4.3±0.4		
N283E	undetectable		
D310A	undetectable		
N323E	undetectable		

Figure 3. Crystal Structure of the LGN TPR2–7-GL34 Fusion Protein

(A) Ribbon diagram representation of TPR2–7-GL34. TPR motifs are colored gold, GL3 is purple, GL4 is magenta, the linker between GL3 and GL4 is green, and the linker between TPR motifs and GL34 is gray.

(B) Stereo view showing the interaction details between TPR2–7 and GL34. Dotted lines denote hydrogen bonds and salt bridge interactions. The double Arg-finger of GL3 and GL4 is colored cyan, where the side chain of the second Arg in GL4 could not observed in the crystal.

(C) Summary of the quantitative binding constants between various forms of TPR0–7 and GL34 fragments used to verify the interaction between TPR0–7 and GL34 observed in the TPR2–7-GL34 structure. All quantitative binding affinities were derived from ITC-based titration assays.

See also Figures S1–S3.

NuMA peptide (aa 1,896–1,912, referred to as the NuMA_C peptide) binds to LGN TPR0–3. Thus, the NuMA_C peptide binding region and the GL34-binding region on LGN TPR motifs do not overlap with each other (Figures S2A–S2C). Consistent with this structural analysis, the interaction between NuMA_C peptide with TPR0–7 was not obviously influenced by the presence of an excess amount of GL34 (Figure S2D). Conversely, the interaction between TPR0–7 with GL34 was only marginally influenced by the presence of the NuMA_C peptide (Figure S2E).

GL/TPR Motif Interactions versus GL/Gα_i·GDP Interactions

It is well known that GL motifs bind to the GDP-bound form Gα subunit of the heterotrimeric G proteins and function as GDIs (Willard et al., 2004; Yu et al., 2005). Comparison of the structures of GL/Gα_i–GDP complexes (Jia et al., 2012; Kimple et al., 2002) with that of LGN TPR2–7-GL34 reveals two distinct target-binding modes of GL motifs (Figure 4). All GL motifs contain a stretch of ~20 continuous and highly conserved residues (Jia et al., 2012; Peterson et al., 2000; Siderovski et al., 1999) (also see Figure 4E). Each individual GL motif can bind to Gα_i·GDP with a binding affinity in the range of tens to hundreds of nM (Jia et al., 2012; Kimple et al., 2002). In the GL/Gα_i·GDP complexes, the N-terminal half of the conserved 20-residue GL motif typically forms an α-helix and binds to the Ras-like domain of Gα_i mainly via hydrophobic interactions (Figures 4A and 4D). The two Arg residues in the second half of the GL motif (the so-called "double Arg-finger" [Jia et al., 2012], Arg635 and Arg640 in GL4 shown in Figure 4D) are chiefly responsible for binding to GDP from Gα_i and thus are essential for the GL/Gα_i·GDP interaction, which is different from the RGS14 GL motif, in which only one Arg is necessary to stabilize GDP (Jia et al., 2012; Kimple et al., 2002). LGN TPR motifs do not bind to GDP. Correspondingly, the "double Arg-finger" sequence of either GL3 or GL4 does not participate in the LGN TPR-motif binding (Figure 3B, 4A, and 4C). There are no direct charge-charge interactions or hydrogen bonds observed for these Arg residues in the crystal packing surfaces (data not shown).The residues that are responsible for GL/TPR motifs binding in both GL3 and GL4 are concentrated in the N-terminal half of the 20-residue GL motif (Figure 4C). As in the GL/Gα_i·GDP complexes, the N-terminal halves of GL3 and GL4 in LGN TPR2–7-GL34 also adopt α-helical structure and bind to the TPR motifs mainly via hydrophobic interactions (Figure 4C). Two GL motifs connected in tandem are required to form a stable complex with TPR motifs, presumably compensating for the binding energy corresponding to the "double Arg-finger"/GDP interaction in the GL/Gα_i·GDP complexes. In addition, the N-terminal conserved negatively charged residues of GL motifs also play a role in binding to TPR motifs. The GL3 α-helix is shorter than the GL4 α-helix in LGN TPR2–7-GL34 (Figures 4A–4C). It is possible that the formation of the intermolecular disulfide bond between TPR2–7-GL34 fusion proteins might have contributed to the early termination of the GL3 α-helix at Cys597 (Figure S1).

Mapping the Binding Site of GL12 on TPR0–7

None of our efforts to obtain crystal structures of the GL12/TPR-motif complexes or TPR-GL12 fusion proteins were successful. To obtain a more complete picture of the intramolecular interaction of LGN, we characterized the GL12/TPR interaction by point mutations under guidance of the TPR2–7-GL34 structure and the sequence alignment between GL12 and GL34 (Figure 5A). As observed in the TPR2–7-GL34, substitution of the conserved Phe residues in the N-terminal half of GL1 (Phe487) or GL2 (Phe539) with Glu abolished the interaction between GL12 and TPR0–7 (Figures 5A and 5B). Substitution of Lys96 in TPR2-αA with Ala dramatically decreased the binding of TPR0–7 to

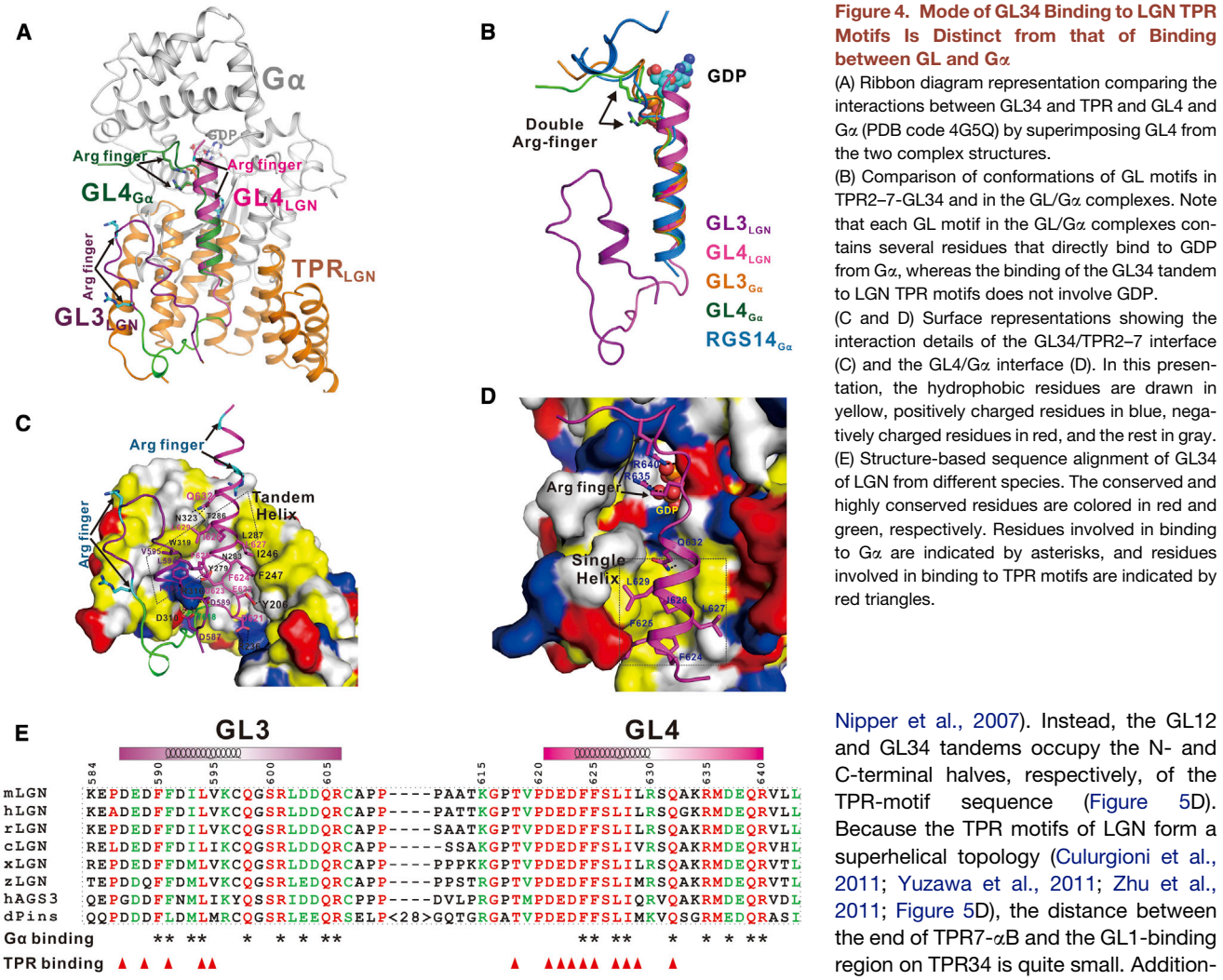

Figure 4. Mode of GL34 Binding to LGN TPR Motifs Is Distinct from that of Binding between GL and Gα

(A) Ribbon diagram representation comparing the interactions between GL34 and TPR and GL4 and Gα (PDB code 4G5Q) by superimposing GL4 from the two complex structures.

(B) Comparison of conformations of GL motifs in TPR2–7-GL34 and in the GL/Gα complexes. Note that each GL motif in the GL/Gα complexes contains several residues that directly bind to GDP from Gα, whereas the binding of the GL34 tandem to LGN TPR motifs does not involve GDP.

(C and D) Surface representations showing the interaction details of the GL34/TPR2–7 interface (C) and the GL4/Gα interface (D). In this presentation, the hydrophobic residues are drawn in yellow, positively charged residues in blue, negatively charged residues in red, and the rest in gray.

(E) Structure-based sequence alignment of GL34 of LGN from different species. The conserved and highly conserved residues are colored in red and green, respectively. Residues involved in binding to Gα are indicated by asterisks, and residues involved in binding to TPR motifs are indicated by red triangles.

GL12, and further substitution of Arg136 in TPR3-αA with Ala (K96, R136A) totally disrupted the TPR0–7/GL12 complex formation, suggesting that TPR motifs 2 and 3 are required for GL12 binding (Figures 5B and 5C). Additionally, substitution of Arg221 in TPR4-αB and Arg236 in TPR5-αA with Ala or Asn203 in TPR4-αA with Glu also abolished the interaction between TPR0–7 and GL12, suggesting that TPR4 and TPR5 are involved in GL12 binding (Figures 5B and 5C). As expected, mutation of residues from TPR6 (Asn283) or TPR7 (Asp310) had no impact on the interaction between TPR0–7 and GL12 (Figure 5B). The above biochemical data, together with the structural details of the TPR4–7/GL34 interaction, suggest that TPR2–4 are primarily responsible for binding to GL12 (Figure 5C). We propose that, analogous to the TPR4–7/GL34 interaction, GL2 and GL1 mainly bind to the TPR23 and TPR34 fragments, respectively (Figure 5C). Based on our biochemical data and structure-based analysis, we made the GL12 model, docked this model into TPR motifs, and, finally, made a schematic model structure of the fully autoinhibited LGN (Figure 5D). It is noted that the TPR motifs and the GL motifs of LGN are not arranged in a simple head-to-tail fashion, as assumed in previous studies (Du and Macara, 2004; Nipper et al., 2007). Instead, the GL12 and GL34 tandems occupy the N- and C-terminal halves, respectively, of the TPR-motif sequence (Figure 5D). Because the TPR motifs of LGN form a superhelical topology (Culurgioni et al., 2011; Yuzawa et al., 2011; Zhu et al., 2011; Figure 5D), the distance between the end of TPR7-αB and the GL1-binding region on TPR34 is quite small. Additionally, the linker region connecting the TPR motifs and the GL motifs contains ~120 residues that are mainly unstructured (our unpublished data). Therefore, the head-to-head interaction between the TPR motifs and the GL motifs of LGN shown in Figure 5D is feasible.

The Intramolecular Interaction of LGN Modulates the Intermolecular Interactions in the NuMA/LGN/$G\alpha_i$ Complex

Previous studies showed that the closed conformation of LGN (Pins) can regulate its interaction with NuMA (Mud) through $G\alpha_i$ (Du and Macara, 2004; Nipper et al., 2007). Here, we characterized this regulation in more detail. First, the interaction between NuMA (aa 1886–1958) and the full-length LGN was assayed in the absence and presence of $G\alpha_i$•GDP. Both analytical gel-filtration-chromatography- and ITC-based assays showed that the LGN/NuMA binding is marginal without the presence of $G\alpha_i$•GDP (Figures 6A, 6B, and 6D). In contrast, in the presence of four molar-equivalent amounts of $G\alpha_i$•GDP (i.e., LGN:NuMA:$G\alpha_i$•GDP = 1:1:4), NuMA was able to form a stable complex with LGN (Figures 6A, 6B, and 6E). The apparent weaker binding of NuMA to the LGN/$G\alpha_i$•GDP mixture (Figure 6E) than the same NuMA to TPR0–7 (Figure 6C) is presumably due to

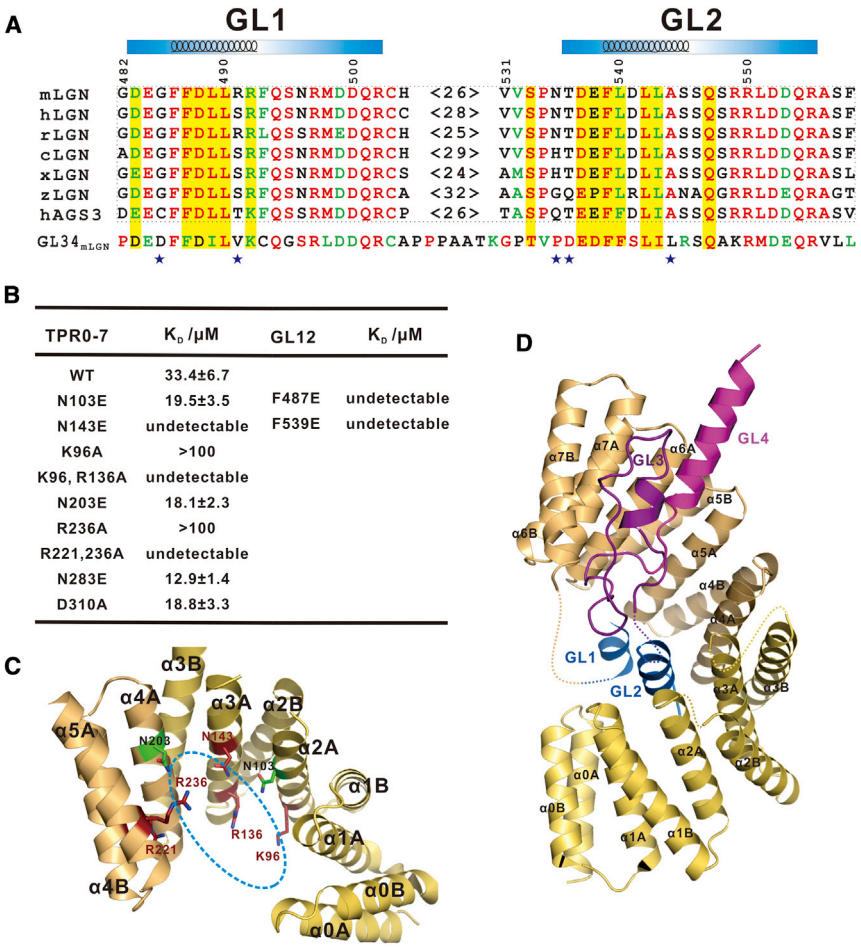

Figure 5. Mapping the Binding Site of GL12 on TPR0–7

(A) Amino acid sequence alignment of GL12 of LGN from different species. The GL12 sequence is also aligned with that of GL34 based on the structure of GL34/TPR2–7. In this alignment, the residues shaded in yellow are conserved between GL12 and GL34 and these residues are found to mediate interaction between GL34 and TPR4–7. The residues indicated with blue stars may determine the TPR0–7 binding specificity of GL12 and GL34, as these residues are critical for the GL34/TPR4–7 interaction but are not conserved between GL12 and GL34.

(B) ITC-derived binding affinities between various fragments of TPR0–7 and GL12.

(C) Mapping of the amino acid residues that are critical for GL12 binding to TPR0–7. The residues in red denote mutations that led to disruption of GL12 binding, and those in green indicate substitutions that did not alter GL12 binding. A tentative GL12 binding surface on LGN TPR motifs, derived from the above analysis, is indicated with a dashed oval.

(D) A structural model showing the fully autoinhibited conformation of LGN TPR0–7 in complex with GL1–GL4.

the incomplete release of the GL motifs from TPR motifs by $G\alpha_i$•GDP. The data in Figure 6 demonstrate that the intramolecular, GL-motif-mediated binding to the TPR motifs can indeed inhibit LGN from binding to its targets, such as NuMA, and that binding of $G\alpha_i$•GDP to the GL motifs would release the autoinhibited conformation of LGN. The data also provide a clear mechanistic explanation of receptor-independent target activity regulation by $G\alpha_i$.

DISCUSSION

LGN (Pins) is a key regulator of cell polarity and spindle orientation during ACD. LGN (Pins) has been shown to serve as a conformational switch that forms a closed structure through intramolecular interactions between its TPR motifs and GL motifs (Du and Macara, 2004; Nipper et al., 2007; Smith and Prehoda, 2011). The crystal structure of TPR2–7-GL34 solved in this work provides structural information regarding the molecular mechanism of GL-mediated autoinhibition of LGN. The four C-terminal GL motifs of LGN form two GL tandems (GL12 and GL34) to bind to TPR0–3 and TPR4–7, respectively, whereas no binding was observed between any single GL motif and the TPR motifs (Figures 1 and 2). These data strongly suggest that two GL motifs connected in tandem represent the minimal TPR-motif-binding unit. This conclusion is consistent with an earlier finding that GL23 of Pins from *Drosophila* is capable of coupling to the TPR motifs, but that the orphan GL1 cannot (Nipper et al., 2007). The fact that Pins only contains three GL motifs, and thus only GL2 and GL3 are involved in the autoinhibition of its TPR motifs, may explain why Pins TPR motifs are only partially inhibited by its GL motifs (Nipper et al., 2007). The presence of four functional GL motifs in LGN presumably allows the occupation of the majority of the eight N-terminal TPR motifs by the two GL tandems, thus leading to stronger autoinhibition. The different binding affinities of GL12 and GL34 to the TPR motifs may also allow a graded regulation of the conformational opening of LGN by $G\alpha_i$•GDP, given that the affinities of each individual GL in binding to $G\alpha_i$•GDP are comparable (Jia et al., 2012; McCudden et al., 2005; Schaefer et al., 2000, 2001).

The autoinhibited conformation of LGN provides a regulatory switch for the bindings of TPR motifs to their targets, including NuMA. As expected, the LGN/NuMA interaction is largely repressed in the absence of $G\alpha_i$·GDP (Figures 6A, 6B, and 6D). However, binding of $G\alpha_i$·GDP to LGN greatly facilitated binding of NuMA to LGN, likely due to the release of the autoinhibition of LGN (Figures 6A, 6B, and 6E). Our structural analysis provides a clear mechanistic explanation for this regulatory switch. The GL34/TPR interaction observed in TPR2–7-GL34 structure represents a distinct binding mode for GL motifs compared to the only other known GL-mediated interaction observed in GL/$G\alpha_i$·GDP complexes (Jia et al., 2012; Kimple et al., 2002). Since at least a pair of GL motifs connected in tandem is required for binding to TPR motifs, we propose that the autoinhibited conformation observed for LGN may also occur

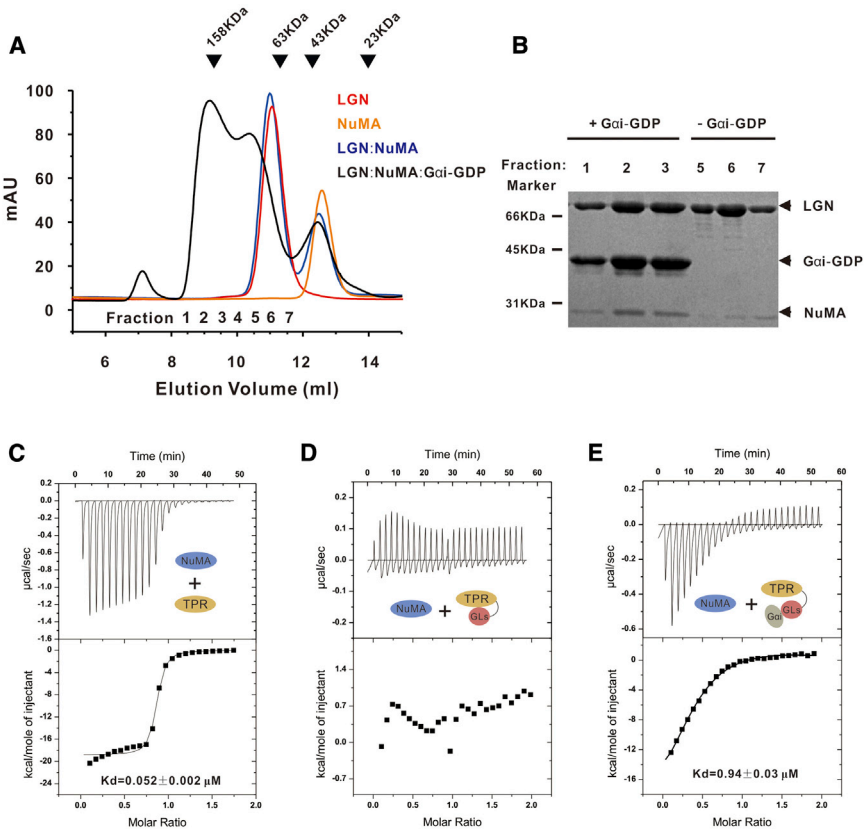

Figure 6. $G\alpha_i$ Can Release the Autoinhibited Conformation of LGN

(A) Analytical gel-filtration elution profiles of the full-length LGN (red); NuMA (orange); an LGN/NuMA mixture (molar ratio 1:1, blue); and an LGN/NuMA/$G\alpha_i$·GDP mixture (molar ratio 1:1:4, black). The extinction coefficients of LGN, NuMA, and $G\alpha_i$ are 54,165, 22,705, and 39,475.

(B) SDS-PAGE analysis of the protein components from the eluted peaks of the LGN/NuMA/$G\alpha_i$·GDP mixture (fraction, 1–3) and the LGN/NuMA mixture (fraction 5–7) in (A). The fraction volume is 0.5 ml.

(C–E) ITC-based measurements of the binding of NuMA to LGN TPR0–7 (C) and to full-length LGN without (D) and with (E) saturating amounts of $G\alpha_i$·GDP.

in other multiple-GL-motif-containing proteins, such as AGS3, PCP2, and GPSM3. In contrast, the GL motif in proteins that containing a single GL motif (e.g., RGS12 and RGS14) is unlikely to bind to target proteins other than $G\alpha_i$·GDP.

The regulation of conformation changes of autoinhibited LGN (also known as G-protein signaling modulator-2) plays essential roles in the receptor-independent G-protein signaling pathway in asymmetric cell divisions. In the canonical signaling mode, extracellular signals can be transduced into cells via GPCR. Ligand-mediated activation of GPCR catalyzes the exchange of GDP for GTP in binding to Gα and subsequently results in the dissociation of Gα·GTP from the Gβγ heterodimer, which in turn act on their respective effectors (Gilman, 1987; Malbon, 2005; Sprang, 1997) (Figure 7A). This ligand-dependent signaling pathway is attenuated by intrinsic GTPase activity of Gα. Recent studies have identified several accessory proteins that regulate the G-protein signaling pathway. For example, each single-GL-motif-containing protein (RGS12 and RGS14) possesses an RGS domain that dramatically accelerates the intrinsic GTPase activity of Gα and thus functions as a GTPase-activating protein (GAP), and a GL motif that binds to the GDP-bound form of Gα to function as a GDI (Kimple et al., 2001; Snow et al., 1998) (Figure 7A). In addition to the ligand-dependent G-protein signaling shown in Figure 7A, multiple GL-motif-containing proteins such as LGN can also conduct ligand-independent G-protein signaling events (Figure 7B). Binding of multiple $G\alpha_i$·GDP to LGN not only localizes LGN to the cell cortex but also releases the autoinhibited conformation of LGN and thereby enables LGN TPR motifs to bind to its effectors (e.g., NuMA). Thus, LGN can serve as a molecular link to tether the cell cortex to the mitotic spindle machinery during asymmetric cell division (Figure 7B). Again, multiple and orphan GL motif-containing proteins are expected to participate in G-protein signaling with distinct mechanisms.

EXPERIMENTAL PROCEDURES

Protein Preparation

The mouse $G\alpha_{i3}$, the full-length LGN, LGN TPR-motif and GL-motif fragments (Figures 1B, 2A, and 2B), fusion proteins (Figures 2A and S2) and mutants (Figures 3D and 5B), and the human NuMA C-terminal fragment (aa 1886–1958) were individually cloned into a modified version of pET32a vector. All the mutations were created using the standard PCR-based method and confirmed by DNA sequencing. Recombinant proteins were expressed in *Escherichia coli* BL21 (DE3) host cells at 16°C and were purified using Ni^{2+}-NTA agarose affinity chromatography followed by size-exclusion chromatography.

Isothermal Titration Calorimetry Assay

ITC measurements were performed on an ITC200 microcalorimeter (MicroCal) at 25°C. All protein samples were in 50 mM Tris (pH 8.0), 100 mM NaCl, and 1 mM EDTA buffer. The protein concentrations used in the cell and in the syringe for each experiment are 0.05 and 0.5 mM, respectively. The titrations were carried out by injecting 10 μl aliquots of the GL-motif fragments into TPR-motif fragments or fusion proteins at time intervals of 2 min to ensure that the titration peak returned to the baseline. The titration data were analyzed using the program Origin7.0 from MicroCal.

Crystallography

Crystals of the TPR2–7-GL34 fusion protein (LGN aa 89–644, in which aa 351–585 are substituted with a PreScission protease LEVLFQGP cleavage site) were obtained by the hanging-drop vapor diffusion method at 18°C. The crystals were grown in buffer containing 0.2 M NaCl, 0.1 M Bis-Tris (pH 5.5), 25% Polyethylene Glycol 3350, and another buffer containing 0.2 M Ammonium Acetate, 0.1 M Bis-Tris (pH 5.5), and 25% Polyethylene Glycol 3350. Crystals were soaked in crystallization solution containing 20% glycerol for cryoprotection. Molecular replacement was used to solve the structure. A 2.8 Å resolution X-ray data set was collected at the beamline BL17U1 of the Shanghai Synchrotron Radiation Facility. The diffraction data were processed and scaled by HKL2000 (Otwinowski and Minor, 1997). Phenix.xtriage (Adams et al., 2010) was used to show that there were pseudotranslational symmetry peaks at (0.5,0.5,0.111). The TPR4–7 motifs from the TPR4–7/mInsc complex structure (PDB code 3RO3) were used to generate a unit of "dimer" by applying the

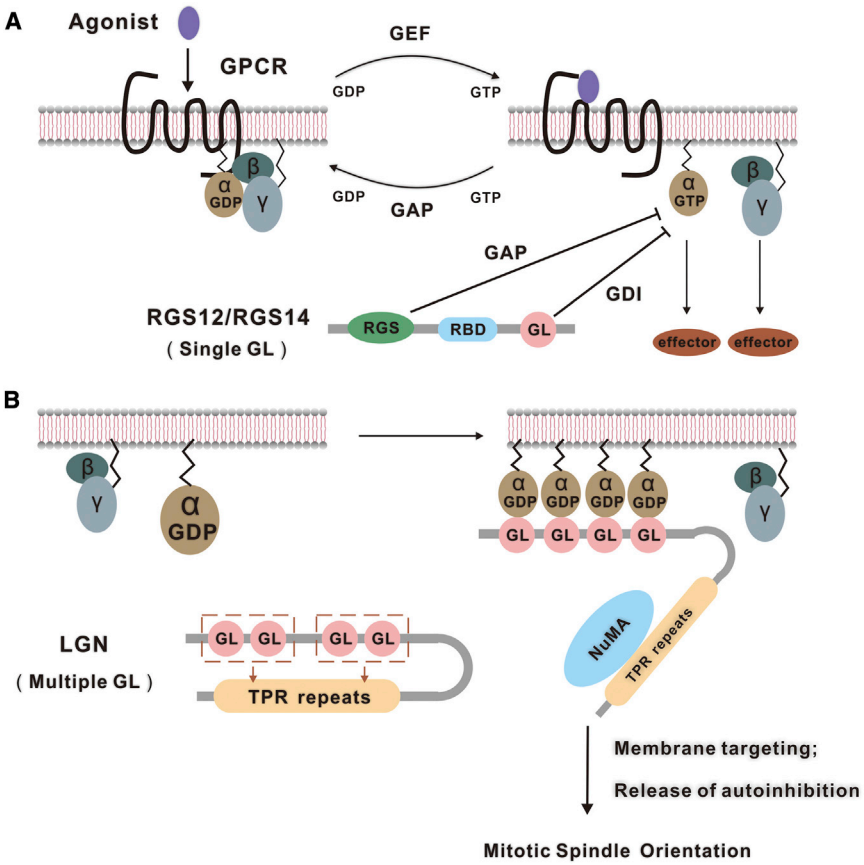

Figure 7. Model Showing G-Protein-Mediated Regulation of LGN Activation

(A) In the canonical G-protein signaling pathway, ligand-mediated activation of GPCR catalyzes the exchange of GDP for GTP in binding to Gα, leading to the dissociation of Gα·GTP from the Gβγ heterodimer, which triggers their respective signal effectors. Single-GL-motif-containing proteins such as RGS12 and RGS14 function as both GAPs and GDIs, which play essential roles in modulating G-protein signaling.

(B) In the receptor-independent G-protein signaling pathway involving LGN, binding of $G\alpha_i$·GDP to LGN not only will recruit LGN to the cell cortex, but will also help LGN to release its autoinhibited conformation, thus facilitating formation of the $G\alpha_i$/LGN/NuMA complex required for proper alignment of mitotic spindles during asymmetric cell division.

pseudotranslational symmetry vector. This unit was used as the search model in molecular replacement using PHASER (McCoy et al., 2007). Further manual model building and adjustment were completed using COOT (Emsley et al., 2010). The model was then refined by the phenix.refinement (Adams et al., 2010). During the refinement, we changed one protein molecule to its crystal symmetry mate to get better refinement statistics (Zwart et al., 2008). The existence of pseudotranslational symmetry in the crystal caused systematically strong and weak reflections at low resolution, and this resulted in relatively higher R factors (for examples, see Poy et al., 2001; Vajdos et al., 1997). The final structure was validated by the phenix.model_vs_data validation tools (Adams et al., 2010). The final refinement statistics are summarized in Table 1.

The LGN Full-Length Model Building

The structure of the GL12 fragment ("^{486}FFDLLRR^{492}" and "^{537}DEFLDLLASSQSR^{549}") was modeled based on the sequence alignment in Figure 5A and TPR/GL34's structure using the program COOT (Emsley et al., 2010). The side chains of residues F486, R491, and R549 were not modeled, as the corresponding residues in GL34 are not directly involved in binding with TPR motifs. The GL12 model was docked onto the TPR1–5 fragment from the TPR0–7 model structure (PDB ID 3RO2) using Hex Protein Docking Webserver (http://hexserver.loria.fr). Among the top 100 results, the best docking result is consistent with our biochemical data. The LGN TPR0–7-GL12-GL34 model was then modeled by superimposing the TPR2–7-GL34 structure, the modeled GL12/TPR1–5 structure, and the TPR0–7 structure (PDB ID 3RO2).

Fluorescence Polarization Assay

Fluorescence assays were performed on a PerkinElmer LS-55 fluorimeter equipped with an automated polarizer at 25°C. Commercial synthesized peptides were labeled with fluorescein-5-isothiocyanate (Invitrogen, Molecular Probe) at N-termini. In a typical assay, the FITC-labeled peptide (~1 μM) was titrated with binding partners in a 50 mM Tris (pH 8.0) buffer containing 100 mM NaCl, 1 mM dithiothreitol, and 1 mM EDTA. The K_d values were obtained by fitting the titration curves with the classical one-site binding model.

ACCESSION NUMBERS

The atomic coordinates of LGN TPR2–7-GL34 have been deposited in the Protein Data Bank under the accession code 4JHR.

SUPPLEMENTAL INFORMATION

Supplemental Information includes three figures and can be found with this article online at http://dx.doi.org/10.1016/j.str.2013.04.005.

ACKNOWLEDGMENTS

We thank the Shanghai Synchrotron Radiation Facility for BL17U1 beamline time. This work was supported by grants from RGC of Hong Kong to M.Z. (663610, 663811, 663812, HKUST6/CRF/10, SEG_HKUST06, and T13-607/12R), the National Major Basic Research Program of China (2009CB918600 and 2011CB808505), the National Science Foundation of China (20973040, 31070642, 30970574, and 31270778), and the Science & Technology Commission of Shanghai Municipality (08DZ2270500). M.Z. is a Kerry Holdings Professor of Science and a Senior Fellow of IAS at Hong Kong University of Science and Technology.

Received: December 21, 2012
Revised: March 11, 2013
Accepted: April 5, 2013
Published: May 9, 2013

REFERENCES

Adams, P.D., Afonine, P.V., Bunkóczi, G., Chen, V.B., Davis, I.W., Echols, N., Headd, J.J., Hung, L.W., Kapral, G.J., Grosse-Kunstleve, R.W., et al. (2010). PHENIX: a comprehensive Python-based system for macromolecular structure solution. Acta Crystallogr. D Biol. Crystallogr. *66*, 213–221.

Bowman, S.K., Neumüller, R.A., Novatchkova, M., Du, Q., and Knoblich, J.A. (2006). The *Drosophila* NuMA Homolog Mud regulates spindle orientation in asymmetric cell division. Dev. Cell *10*, 731–742.

Couwenbergs, C., Labbé, J.C., Goulding, M., Marty, T., Bowerman, B., and Gotta, M. (2007). Heterotrimeric G protein signaling functions with dynein to promote spindle positioning in *C. elegans*. J. Cell Biol. *179*, 15–22.

Cowan, C.R., and Hyman, A.A. (2004). Asymmetric cell division in *C. elegans*: cortical polarity and spindle positioning. Annu. Rev. Cell Dev. Biol. *20*, 427–453.

Culurgioni, S., Alfieri, A., Pendolino, V., Laddomada, F., and Mapelli, M. (2011). Inscuteable and NuMA proteins bind competitively to Leu-Gly-Asn repeat-enriched protein (LGN) during asymmetric cell divisions. Proc. Natl. Acad. Sci. USA *108*, 20998–21003.

Du, Q., and Macara, I.G. (2004). Mammalian Pins is a conformational switch that links NuMA to heterotrimeric G proteins. Cell *119*, 503–516.

Emsley, P., Lohkamp, B., Scott, W.G., and Cowtan, K. (2010). Features and development of Coot. Acta Crystallogr. D Biol. Crystallogr. *66*, 486–501.

Gilman, A.G. (1987). G proteins: transducers of receptor-generated signals. Annu. Rev. Biochem. *56*, 615–649.

Gönczy, P. (2008). Mechanisms of asymmetric cell division: flies and worms pave the way. Nat. Rev. Mol. Cell Biol. *9*, 355–366.

Izumi, Y., Ohta, N., Hisata, K., Raabe, T., and Matsuzaki, F. (2006). *Drosophila* Pins-binding protein Mud regulates spindle-polarity coupling and centrosome organization. Nat. Cell Biol. *8*, 586–593.

Jia, M., Li, J., Zhu, J., Wen, W., Zhang, M., and Wang, W. (2012). Crystal structures of the scaffolding protein LGN reveal the general mechanism by which GoLoco binding motifs inhibit the release of GDP from Gαi. J. Biol. Chem. *287*, 36766–36776.

Kimple, R.J., De Vries, L., Tronchère, H., Behe, C.I., Morris, R.A., Gist Farquhar, M., and Siderovski, D.P. (2001). RGS12 and RGS14 GoLoco motifs are G α_i interaction sites with guanine nucleotide dissociation inhibitor activity. J. Biol. Chem. *276*, 29275–29281.

Kimple, R.J., Kimple, M.E., Betts, L., Sondek, J., and Siderovski, D.P. (2002). Structural determinants for GoLoco-induced inhibition of nucleotide release by Gα subunits. Nature *416*, 878–881.

Knoblich, J.A. (2010). Asymmetric cell division: recent developments and their implications for tumour biology. Nat. Rev. Mol. Cell Biol. *11*, 849–860.

Kotak, S., Busso, C., and Gönczy, P. (2012). Cortical dynein is critical for proper spindle positioning in human cells. J. Cell Biol. *199*, 97–110.

Malbon, C.C. (2005). G proteins in development. Nat. Rev. Mol. Cell Biol. *6*, 689–701.

McCoy, A.J., Grosse-Kunstleve, R.W., Adams, P.D., Winn, M.D., Storoni, L.C., and Read, R.J. (2007). Phaser crystallographic software. J. Appl. Cryst. *40*, 658–674.

McCudden, C.R., Willard, F.S., Kimple, R.J., Johnston, C.A., Hains, M.D., Jones, M.B., and Siderovski, D.P. (2005). Gα selectivity and inhibitor function of the multiple GoLoco motif protein GPSM2/LGN. Biochim. Biophys. Acta *1745*, 254–264.

Merdes, A., Ramyar, K., Vechio, J.D., and Cleveland, D.W. (1996). A complex of NuMA and cytoplasmic dynein is essential for mitotic spindle assembly. Cell *87*, 447–458.

Morrison, S.J., and Kimble, J. (2006). Asymmetric and symmetric stem-cell divisions in development and cancer. Nature *441*, 1068–1074.

Neumüller, R.A., and Knoblich, J.A. (2009). Dividing cellular asymmetry: asymmetric cell division and its implications for stem cells and cancer. Genes Dev. *23*, 2675–2699.

Nguyen-Ngoc, T., Afshar, K., and Gönczy, P. (2007). Coupling of cortical dynein and Gα proteins mediates spindle positioning in *Caenorhabditis elegans*. Nat. Cell Biol. *9*, 1294–1302.

Nipper, R.W., Siller, K.H., Smith, N.R., Doe, C.Q., and Prehoda, K.E. (2007). $G\alpha_i$ generates multiple Pins activation states to link cortical polarity and spindle orientation in *Drosophila* neuroblasts. Proc. Natl. Acad. Sci. USA *104*, 14306–14311.

Otwinowski, Z., and Minor, W. (1997). Processing of X-ray diffraction data collected in oscillation mode. Methods Enzymol. *276*, 307–326.

Park, D.H., and Rose, L.S. (2008). Dynamic localization of LIN-5 and GPR-1/2 to cortical force generation domains during spindle positioning. Dev. Biol. *315*, 42–54.

Parmentier, M.L., Woods, D., Greig, S., Phan, P.G., Radovic, A., Bryant, P., and O'Kane, C.J. (2000). Rapsynoid/partner of inscuteable controls asymmetric division of larval neuroblasts in *Drosophila*. J. Neurosci. *20*, RC84.

Peterson, Y.K., Bernard, M.L., Ma, H., Hazard, S., 3rd, Graber, S.G., and Lanier, S.M. (2000). Stabilization of the GDP-bound conformation of Giα by a peptide derived from the G-protein regulatory motif of AGS3. J. Biol. Chem. *275*, 33193–33196.

Poy, F., Lepourcelet, M., Shivdasani, R.A., and Eck, M.J. (2001). Structure of a human Tcf4-β-catenin complex. Nat. Struct. Biol. *8*, 1053–1057.

Schaefer, M., Shevchenko, A., Shevchenko, A., and Knoblich, J.A. (2000). A protein complex containing Inscuteable and the Gα-binding protein Pins orients asymmetric cell divisions in *Drosophila*. Curr. Biol. *10*, 353–362.

Schaefer, M., Petronczki, M., Dorner, D., Forte, M., and Knoblich, J.A. (2001). Heterotrimeric G proteins direct two modes of asymmetric cell division in the *Drosophila* nervous system. Cell *107*, 183–194.

Siderovski, D.P., Diversé-Pierluissi, Ma., and De Vries, L. (1999). The GoLoco motif: a $G\alpha_i/o$ binding motif and potential guanine-nucleotide exchange factor. Trends Biochem. Sci. *24*, 340–341.

Siller, K.H., and Doe, C.Q. (2008). Lis1/dynactin regulates metaphase spindle orientation in *Drosophila* neuroblasts. Dev. Biol. *319*, 1–9.

Siller, K.H., and Doe, C.Q. (2009). Spindle orientation during asymmetric cell division. Nat. Cell Biol. *11*, 365–374.

Siller, K.H., Serr, M., Steward, R., Hays, T.S., and Doe, C.Q. (2005). Live imaging of *Drosophila* brain neuroblasts reveals a role for Lis1/dynactin in spindle assembly and mitotic checkpoint control. Mol. Biol. Cell *16*, 5127–5140.

Siller, K.H., Cabernard, C., and Doe, C.Q. (2006). The NuMA-related Mud protein binds Pins and regulates spindle orientation in *Drosophila* neuroblasts. Nat. Cell Biol. *8*, 594–600.

Smith, N.R., and Prehoda, K.E. (2011). Robust spindle alignment in *Drosophila* neuroblasts by ultrasensitive activation of pins. Mol. Cell *43*, 540–549.

Snow, B.E., Hall, R.A., Krumins, A.M., Brothers, G.M., Bouchard, D., Brothers, C.A., Chung, S., Mangion, J., Gilman, A.G., Lefkowitz, R.J., and Siderovski, D.P. (1998). GTPase activating specificity of RGS12 and binding specificity of an alternatively spliced PDZ (PSD-95/Dlg/ZO-1) domain. J. Biol. Chem. *273*, 17749–17755.

Sprang, S.R. (1997). G protein mechanisms: insights from structural analysis. Annu. Rev. Biochem. *66*, 639–678.

Vajdos, F.F., Yoo, S., Houseweart, M., Sundquist, W.I., and Hill, C.P. (1997). Crystal structure of cyclophilin A complexed with a binding site peptide from the HIV-1 capsid protein. Protein Sci. *6*, 2297–2307.

Willard, F.S., Kimple, R.J., and Siderovski, D.P. (2004). Return of the GDI: the GoLoco motif in cell division. Annu. Rev. Biochem. *73*, 925–951.

Williams, S.E., Beronja, S., Pasolli, H.A., and Fuchs, E. (2011). Asymmetric cell divisions promote Notch-dependent epidermal differentiation. Nature *470*, 353–358.

Yingling, J., Youn, Y.H., Darling, D., Toyo-Oka, K., Pramparo, T., Hirotsune, S., and Wynshaw-Boris, A. (2008). Neuroepithelial stem cell proliferation requires LIS1 for precise spindle orientation and symmetric division. Cell *132*, 474–486.

Yu, F., Wang, H., Qian, H., Kaushik, R., Bownes, M., Yang, X., and Chia, W. (2005). Locomotion defects, together with Pins, regulates heterotrimeric

G-protein signaling during *Drosophila* neuroblast asymmetric divisions. Genes Dev. *19*, 1341–1353.

Yu, F.W., Kuo, C.T., and Jan, Y.N. (2006). *Drosophila* neuroblast asymmetric cell division: recent advances and implications for stem cell biology. Neuron *51*, 13–20.

Yuzawa, S., Kamakura, S., Iwakiri, Y., Hayase, J., and Sumimoto, H. (2011). Structural basis for interaction between the conserved cell polarity proteins Inscuteable and Leu-Gly-Asn repeat-enriched protein (LGN). Proc. Natl. Acad. Sci. USA *108*, 19210–19215.

Zhu, J., Wen, W., Zheng, Z., Shang, Y., Wei, Z., Xiao, Z., Pan, Z., Du, Q., Wang, W., and Zhang, M. (2011). LGN/mInsc and LGN/NuMA complex structures suggest distinct functions in asymmetric cell division for the Par3/mInsc/LGN and Gαi/LGN/NuMA pathways. Mol. Cell *43*, 418–431.

Zwart, P.H., Grosse-Kunstleve, R.W., Lebedev, A.A., Murshudov, G.N., and Adams, P.D. (2008). Surprises and pitfalls arising from (pseudo)symmetry. Acta Crystallogr. D Biol. Crystallogr. *64*, 99–107.